

# Effect of crystal anisotropy and adhesive forces on laser induced deformation patterns in covalently bonded thin films

D. Walgraef<sup>1</sup> and N. M. Ghoniem<sup>2</sup><sup>1</sup>Center of Nonlinear Phenomena and Complex Systems, Free University of Brussels, CP 231, Boulevard du Triomphe, B-1050 Brussels, Belgium<sup>2</sup>Mechanical and Aerospace Engineering Department, The University of California at Los Angeles, Los Angeles, California 90024  
(Received 8 May 2001; published 25 March 2002)

The effect of crystal structure on laser induced deformation patterns in thin films and surfaces is analyzed within the framework of a dynamical model for the coupled evolution of defect densities and deformation fields. In crystals with covalent bonding, such as Si and SiC, preferential bond breaking may occur, as a result of the relative orientation of the laser electric field and crystallographic axes. We extend here our theoretical framework to incorporate the effects of anisotropic defect diffusion, and the influence of film-substrate adhesion on deformation pattern selection and stability of thin films subjected to laser beams. We also compare theoretical predictions to experimental observations on single crystal silicon wafer surfaces. Furthermore, it is predicted that the laser induced damage threshold for SiC single crystals can be in excess of 200 J/cm<sup>2</sup>.

DOI: 10.1103/PhysRevB.65.155304

PACS number(s): 81.65.-b, 61.80.Az, 62.20.Fe, 68.43.-h

## I. INTRODUCTION

Many irreversible structural and morphological changes in materials interacting with strong laser beams of energy density  $F \leq F_m$ , where  $F_m$  is the melting threshold, are experimentally observed. Recent experimental investigations revealed phenomena such as the gradual and catastrophic degradation of light-emitting devices,<sup>1</sup> cumulative laser damage to optical components,<sup>2</sup> nonuniform melting of semiconductor surfaces, ultrafast laser-induced phase transitions,<sup>3-5</sup> and various material restructuring phenomena in the material processing field.<sup>6-8</sup> The time of laser-matter interaction, which results in permanent structural changes in materials, can vary from tens of picoseconds to minutes, depending on the value of  $F$ , material conditions, and laser irradiation mode. These changes are desirable in some technological applications (e.g., material processing), or undesirable in others (as in laser reflective mirrors). Laser induced instabilities are becoming particularly important in thin film behavior, coatings, semiconductor surfaces, cumulative laser induced damage (LID) of optical components, etc.<sup>9,11-14</sup> Laser annealing and laser assisted thin film deposition processes also provide numerous examples of such instabilities.<sup>15</sup> Under conditions of interband absorption, semiconductors form defect centers already at laser energy densities  $F = (0.05 - 0.1)F_m$ .<sup>16</sup> Their formation mechanisms are not completely determined, but include heating, acoustic deformation and local electronic excitation of the subsurface layer. In many cases, one may observe the formation of regular structures on the surface of the material, and laser-surface interaction is evidently at the origin of such patterning phenomena.

A common instability mechanism in laser irradiated materials results from the coupling between defect dynamics and surface deformation.<sup>17</sup> The interaction of electromagnetic laser radiation with thin films leads to very strong absorption of photon energy in a shallow layer that is a few wavelengths deep from the surface. As a result, substantial nonequilibrium concentration of lattice defects are generated.

The type of lattice defects depends on photon energy, wavelength of laser radiation, and materials parameters. Examples of such defects are electron-hole pairs in strongly absorbing semiconductors, interstitials and vacancies in thin films, and voids and dislocation loops in prolonged irradiation. It is the coupling between defect generation, diffusion and the deformation field which leads to pattern forming instabilities. As a result, the dynamical description of such phenomena should be based on the dynamics of the defect field  $N_d$  in the thin film and the elastic continuum of the host material described by the displacement vector  $\mathbf{U}(\mathbf{r}, t) = (U_x, U_y, U_z)$  with appropriate boundary conditions, both dynamics being coupled through the defect-strain interaction. Various types of defect structures may be induced by such dynamical systems. For example, in the case of thin films under laser irradiation, regular deformation patterns may appear on the film surface when the laser intensity exceeds some threshold. In spatially extended irradiation zones, one- and two-dimensional gratings have been widely observed.<sup>18,19</sup>

The system to be considered in this case is a thin film on a substrate, which is modeled by a thin horizontal crystalline layer subjected to a transverse laser beam. The geometry of the corresponding setup is represented in Fig. 1. Due to laser-

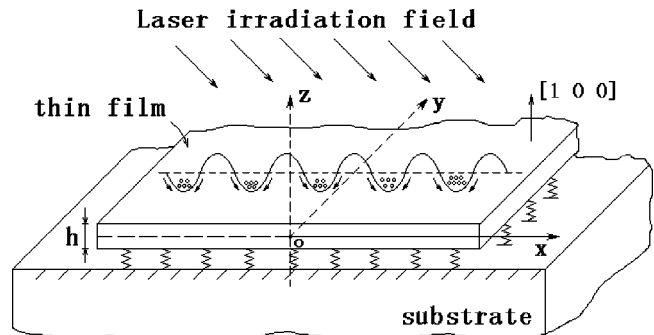


FIG. 1. Geometry of the thin film-substrate system subjected to a uniform laser beam, showing a schematic illustration of the proposed surface deformation mechanism.

induced thermal heating, an increased vacancy density is created in the subsurface layer. The corresponding transverse vacancy density profile results in a body force on the film which may induce bending deformation. Even under uniform irradiation, this system may become unstable versus nonuniform deformations or vacancy density variations. Physically, a local increase in the vacancy density generates lattice contraction in the film. This contraction has two effects: it locally reduces the defect formation energy, and, furthermore, induces a converging defect flux. As a result, both film contraction and local defect density will increase. On the other hand, a deformation bump in the film locally decreases the defect density. It furthermore increases the defect formation energy and induces an outgoing defect flux. In this case, a deformation bump will increase while the defect density will decrease. There is thus a feedback loop between local deformation and defect density variations, which provides a destabilizing mechanism for uniform deformations. However, vacancy diffusion tends to wash out nonuniformities in the system and provides a stabilizing mechanism for uniform defect densities. Instability occurs when the feedback loop effects dominate over diffusion.<sup>17</sup> The growth of this instability is limited by two mechanisms. The first one comes from finite deformation elasticity which limits the growth of the deformation. The second one results from vacancy dynamics, where the extra defect flux induced by surface deformation is proportional to the vacancy density. Consequently, defect fluxes from regions of decreasing defect density decrease accordingly in a feedback process which thus limits defect localization.

All these aspects have been analyzed elsewhere, and assembled in a full dynamical model, able to describe the main features of deformation patterning under laser irradiation.<sup>9,20</sup> This model is based on the following.

(i) A nonuniform laser-induced temperature field across the film.

(ii) The evolution of vacancy density in strained crystals, including generation and transport.

(iii) The deformation of a thin film in the presence of a nonuniform vacancy density. Pattern formation under extended and focused irradiation has already been described elsewhere, in the framework of this model.<sup>9,20,21</sup> However, in these papers, defect generation and transport have been considered as isotropic, which is not applicable for crystals with strong covalent bonding. For example, deformation patterns formed on Si surfaces depend on the laser field orientation in relation to crystallographic axes.<sup>18,19,17</sup> This effect is of practical importance, since the corresponding defect accumulation induces a local decrease in the melting temperature, and can also influence the laser induced damage threshold (LIDT).<sup>22,23</sup>

Another effect that may be of importance for deformation patterns on semiconductor films is the adhesion between the film and its substrate, which may stabilize the film and oppose the development of deformation patterns. It would thus be important to determine, for a given film-substrate system with given adhesive forces, what irradiation intensity is needed to induce instability. On the other hand, it would be interesting to know what adhesive force levels are required

to suppress the surface deformation instability, under given irradiation conditions.

Hence, this paper is devoted to the study the influence of film crystalline anisotropy and film-substrate adhesion effects on laser induced deformation patterns on semiconductor surfaces. This study is performed within the framework of the dynamical model analyzed in Ref. 9, where unsupported, or weakly adherent, isotropic films were considered. The dynamical model and instability conditions for anisotropic films on substrates are presented in Secs. II and III. Post-bifurcation pattern selection and stability are discussed in Sec. IV, where a comparison with experimental observations is also considered. Finally, conclusions are drawn in Sec. VI.

## II. THE DYNAMICAL MODEL

Consider a covalent semiconductor film, such as Si, with its surface oriented along (100) planes, of thickness  $h$ , and irradiated by laser light incident on the surface. Its aspect ratio is large, i.e., the lateral dimensions (corresponding to the  $x$  and  $y$  directions) are much larger than the thickness, as can be seen in Fig. 1. Its dynamics is governed by coupled evolution equations for vacancy density  $C$  and its neutral plane transverse deflection  $\xi$ .<sup>17,9</sup> The kinetic equation for vacancy density may be written as

$$\partial_t C = \vec{\nabla}_{\parallel} \bar{D}_{\parallel} \vec{\nabla}_{\parallel} C - \frac{C}{\tau} + \vec{\nabla}_{\parallel} \frac{\theta_v \bar{D}_{\parallel} C}{kT} \vec{\nabla}_{\parallel} (\vec{\nabla} \mathbf{U}) + g \exp \left[ - \frac{E_f - \theta_v \vec{\nabla} \mathbf{U}}{kT} \right], \quad (1)$$

where  $C = C(x, y, z, t)$ ,  $\vec{\nabla}_{\parallel} = \nabla_x \vec{I}_x + \nabla_y \vec{I}_y$ , and  $\bar{D}_{\parallel}$  is the diffusion tensor along the surface. Diffusion along the  $z$  direction is neglected, since ‘‘bulk’’ diffusion is much slower than surface diffusion (in usual experimental conditions  $D_{\parallel} \tau \approx 10^{-5} \text{ cm}^2$  and  $|\theta_v| \approx 10^{-10} \text{ erg}$ ).<sup>17,18</sup> The displacement vector  $\vec{\mathbf{U}}$  and the deflection of the film’s neutral surface  $\xi$  are related by

$$\vec{\nabla} \cdot \vec{\mathbf{U}} = -z m \Delta \xi, \quad (2)$$

Here,  $z$  is the vertical distance away from the neutral surface  $m = (1 - 2\nu)/(1 - \nu)$ , where  $\nu$  is Poisson’s coefficient. The equilibrium equation for film bending in the presence of a transverse vacancy density gradient and a film-substrate adhesion force may be written as<sup>9</sup>

$$\partial_t^2 \xi + \frac{c^2 h^2}{12} \Delta^2 \xi - \frac{c^2}{2} \sigma_{ij} \partial_{ij}^2 \xi = \frac{\theta_v}{\rho h} (C_+ - C_-) + \frac{F(\xi)}{\rho h}, \quad (3)$$

where  $C_{\pm} = C(x, y, \pm h/2, t)$  and  $F(\xi)$  is the adhesive force per surface unit, between film and substrate. The force of adhesion between the bottom surface of the film and the top layer will be represented by the universal bonding curve, usually invoked in process zone fracture models.<sup>24-26</sup> Figure 2 shows a schematic representation of the universal bonding curve, where the restoring force per unit area on the film’s

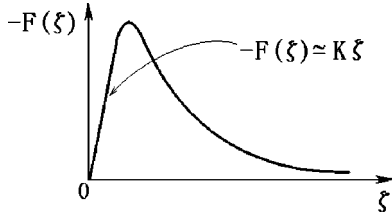


FIG. 2. The universal bonding curve for adhesion between the thin film and substrate. For small film displacements, the force-displacement relationship can be assumed to be linear.

bottom surface is  $F(\xi)$ . Since the film's instability threshold is governed by the small displacement part of the  $F(\xi)$  function, we will approximate it here as  $F(\xi) = -K\xi$ , where  $K$  is the adhesive bond stiffness constant.

Furthermore, the in-plane stress tensor components are related to the film's transverse deflection  $\xi$  as<sup>27</sup>

$$\sigma_{xx} \approx [(\partial_x \xi)^2 + \nu(\partial_y \xi)^2], \quad (4)$$

$$\sigma_{yy} \approx [(\partial_y \xi)^2 + \nu(\partial_x \xi)^2], \quad (5)$$

$$\sigma_{xy} \approx -2(1-\nu)(\partial_x \xi)(\partial_y \xi). \quad (6)$$

All kinetic coefficients and parameters are defined in Ref. 9.

### III. INSTABILITY OF UNDEFORMED STATES

#### A. Unsupported or weakly adherent films

Let us consider the ideal situation of horizontally uniform irradiation of the film surface, which may adequately represent the case of thin films irradiated over a large area by  $cw$  or a pulsed laser source. We will furthermore assume that the adhesive forces are negligible, and that the temperature profile has reached its equilibrium condition, or that its evolution is sufficiently slow, as compared to vacancy generation, to consider it as quasistationary. In the absence of deformation, the equilibrium vacancy density profile  $C^0(z)$  is then the solution of the steady state equation

$$\partial_t C^0 = -\frac{1}{\tau} C^0 + g \exp\left[-\frac{E_f}{kT(z)}\right]. \quad (7)$$

Hence, the transverse variation of the defect density follows the temperature variation across the film. Let us consider strong absorbing layers such that the linear dimension of the irradiated domain is much larger than the film thickness. The temperature profile across the film may then be approximated by<sup>9</sup>

$$T = T_+ + \frac{T_+ - T_-}{h} \left(z - \frac{h}{2}\right) \quad (8)$$

with  $-h/2 < z < h/2$ , and where  $T_+$  and  $T_-$  are the temperatures of upper and lower surfaces, respectively, and  $C^0(z)$  behaves as

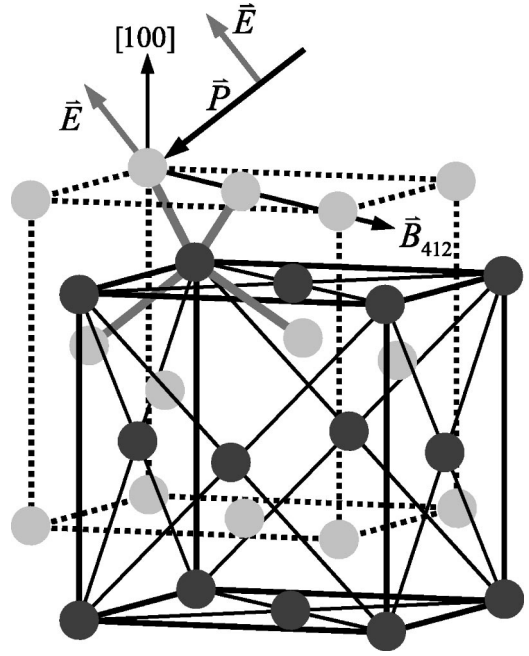


FIG. 3. Si crystal structure showing orientational relationships between the electric field and bond vectors.

$$C^0(z) \approx C_+^0 \exp\left[\gamma\left(z - \frac{h}{2}\right)\right], \quad (9)$$

where  $C_+^0 = g\tau \exp[-E_f/kT_+]$ , when  $\gamma\sqrt{D_1}\tau \ll 1$ , with  $\gamma = E_f\Delta T/kT_+^2h$ . This gives

$$C^0(h/2) = C_+^0, \quad C^0(-h/2) = C_+^0 e^{-\gamma h} = C_-^0. \quad (10)$$

The stability of the undeformed reference state versus spatial perturbations in the horizontal plane may be performed by studying the linear evolution of small perturbations of the undeformed state. Such perturbations are defined as  $n(\vec{r}, z, t) = C(\vec{r}, z, t) - C^0(z)$  or, in particular,  $n_+(\vec{r}, t) = C_+ - C_+^0$  and  $n_-(\vec{r}, t) = C_- - C_+^0 \exp[-\gamma h]$ .

Before deriving linear evolution equations for these perturbations, let us propose explicit expressions for vacancy diffusion appropriate to the case of covalent semiconductors such as Si and SiC. Consider that the (100) surface of a Si or SiC film is irradiated with a linearly polarized laser field with its electric field making an angle  $\alpha$  with the surface. Thus, the Poynting vector makes an angle  $\beta = \pi/2 - \alpha$  with the surface, and when irradiation has normal incidence, the electric field is parallel to it. Since the interaction between the electric field and atomic bonds depends on their relative orientation, one has to analyze how this can affect surface deformation. First, let us recall that Si and SiC are covalent semiconductors, which crystallize in the same structure as diamond, i.e., into a structure formed by two interpenetrating fcc lattices, as represented in Fig. 3.

One sees that there are two families of covalent bonds, which are parallel to (110) planes ( $1=4$  and  $1=2$  bonds) and  $(1\bar{1}0)$  planes ( $1=3$  and  $1=5$  bonds), respectively. It is known from the study of elementary molecular bonds such

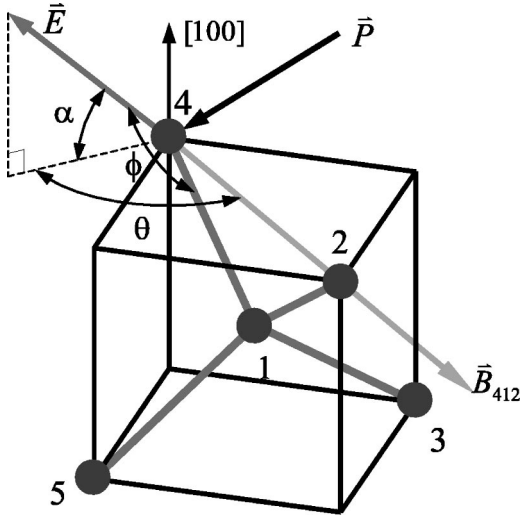


FIG. 4. Coordinate system for the computation of the interaction forces between the electric field and covalent bonds in a Si or SiC elementary cell.

as in  $H_2$  or  $H_2O$ , that the electric field may induce electronic transitions from lower bonding states to upper antibonding states, which effectively corresponds to bond breaking. The interaction force between atomic bonds and the electric field is proportional to the projection of the electric field on the atomic bond direction. On extending this result to Si and SiC covalent bonds, the force constant of the bond is reduced by a factor proportional to  $\cos^2 \phi$ , where  $\phi$  is the angle between the electric field and the atomic bond.<sup>10</sup>

This affects point defect generation and motion in the material. Effectively, if a point defect is present in the vicinity of one of these bonds, its jump probability from one equilibrium state to another, via a saddle point, may be expressed as follows, in the absence of irradiation, for a jump in the  $4=1=2$  direction

$$P_{412}(0) \propto \exp\left(-\frac{H_{41}}{kT}\right), \quad (11)$$

where  $H_{41}$  is proportional to the force constant of the  $4=1$  atomic bond [in fact, without irradiation,  $P_{412}(0) = P_{214}(0) = P_{315}(0) = P_{513}(0) = P(0)$ ].

Under irradiation, this probability increases to

$$P_{412}(\vec{E}) = P(0) \exp\left(\frac{\vartheta E^2 \cos^2 \phi}{kT}\right), \quad (12)$$

where  $\vartheta$  is a proportionality factor, which depends on the microscopic properties of the bond. Let us now compute the various jump probabilities for electric fields making an angle  $\alpha$  with (100) planes and  $\theta$  with (110) planes, within the coordinate system defined in Fig. 4. The electric field may be written as  $\vec{E} = E \sin \alpha \vec{1}_z + E \cos \alpha \cos(3\pi/4 + \theta) \vec{1}_x + E \cos \alpha \sin(3\pi/4 + \theta) \vec{1}_y$ . Hence, the scalar products between the electric field and  $1=2$  and  $1=4$  bonds are  $(Ea/4\sqrt{3})(\sin \alpha - \sqrt{2} \cos \alpha \cos \theta)$  and  $(Ea/4\sqrt{3})(\sin \alpha + \sqrt{2} \cos \alpha \cos \theta)$ , respectively. Similarly, the scalar products between the electric field and  $1=3$  and  $1=5$  bonds are

$-(Ea/4\sqrt{3})(\sin \alpha + \sqrt{2} \cos \alpha \sin \theta)$  and  $-(Ea/4\sqrt{3})(\sin \alpha - \sqrt{2} \cos \alpha \sin \theta)$ , respectively.

As a result, the corresponding jump probabilities become

$$P_{412}(\vec{E}) = P(0) \exp\left[\frac{\varpi E^2}{kT} (\sin^2 \alpha + 2 \cos^2 \alpha \cos^2 \theta - \sqrt{2} \sin 2\alpha \cos \theta)\right],$$

$$P_{214}(\vec{E}) = P(0) \exp\left[\frac{\varpi E^2}{kT} (\sin^2 \alpha + 2 \cos^2 \alpha \cos^2 \theta + \sqrt{2} \sin 2\alpha \cos \theta)\right],$$

$$P_{513}(\vec{E}) = P(0) \exp\left[\frac{\varpi E^2}{kT} (\sin^2 \alpha + 2 \cos^2 \alpha \sin^2 \theta + \sqrt{2} \sin 2\alpha \sin \theta)\right],$$

$$P_{315}(\vec{E}) = P(0) \exp\left[\frac{\varpi E^2}{kT} (\sin^2 \alpha + 2 \cos^2 \alpha \sin^2 \theta - \sqrt{2} \sin 2\alpha \sin \theta)\right], \quad (13)$$

where  $\varpi = (a^2/48) \vartheta$ ,  $a$  being the Si or SiC lattice constant.

For normal irradiation  $\alpha=0$  and

$$P_{412}(\vec{E}) = P_{214}(\vec{E}) = P(0) \exp\left[\frac{2\varpi E^2}{3kT} \cos^2 \theta\right],$$

$$P_{513}(\vec{E}) = P_{315}(\vec{E}) = P(0) \exp\left[\frac{2\varpi E^2}{3kT} \sin^2 \theta\right]. \quad (14)$$

The in-plane diffusion flux can be written as

$$\vec{j} = D_x \nabla_x \vec{1}_x + D_y \nabla_y \vec{1}_y, \quad (15)$$

where  $D_x = D_{\parallel} d_x$ ,  $D_y = D_{\parallel} d_y$ , with  $D_{\parallel} \propto P_0 \exp[2\varpi E^2/3kT]$  and

$$d_x = \exp\left[-\frac{2\varpi E^2}{3kT} \sin^2 \theta\right],$$

$$d_y = \exp\left[-\frac{2\varpi E^2}{3kT} \cos^2 \theta\right], \quad (16)$$

where  $\cos \theta = (\vec{1}_x \cdot \vec{E})/|\vec{E}|$  and  $\sin \theta = (\vec{1}_y \cdot \vec{E})/|\vec{E}|$ .

On performing the following scalings:

$$\partial_T = \tau \partial_t, \quad \bar{\Delta} = \tau D_{\parallel} \Delta, \quad \mu = \frac{6m\theta_v^2 D_{\parallel} \tau}{\rho c^2 h^2 k},$$

$$\beta = \frac{ch}{\sqrt{12} D_{\parallel}}, \quad \xi = \frac{h\theta_v}{2k D_{\parallel} \tau} \xi,$$

$$N = \mu(n_+ + n_-), \quad n = \mu(n_+ - n_-),$$

$$\epsilon = \mu \left( \frac{C_+}{T_+} + \frac{C_-}{T_-} \right), \quad \eta = \mu \left( \frac{C_+}{T_+} - \frac{C_-}{T_-} \right) \quad (17)$$

the dynamical model becomes

$$\partial_T N = (d_x \bar{\nabla}_x^2 + d_y \bar{\nabla}_y^2) N - N - \eta (d_x \bar{\nabla}_x^2 + d_y \bar{\nabla}_y^2 + 1) \bar{\Delta} \zeta$$

$$- [d_x \bar{\nabla}_x (\chi n + \delta N) \bar{\nabla}_x + d_y \bar{\nabla}_y (\chi n + \delta N) \bar{\nabla}_y] \bar{\Delta} \zeta, \quad (18)$$

$$\partial_T n = (d_x \bar{\nabla}_x^2 + d_y \bar{\nabla}_y^2) n - n - \epsilon (d_x \bar{\nabla}_x^2 + d_y \bar{\nabla}_y^2 + 1) \bar{\Delta} \zeta$$

$$- [d_x \bar{\nabla}_x (\chi N + \delta n) \bar{\nabla}_x + d_y \bar{\nabla}_y (\chi N + \delta n) \bar{\nabla}_y] \bar{\Delta} \zeta, \quad (19)$$

$$\frac{1}{\beta^2} \partial_T^2 \zeta = -\bar{\Delta}^2 \zeta + u \sigma_{ij}(\zeta) \bar{\partial}_{ij}^2 \zeta - n + F(\zeta), \quad (20)$$

where  $u = 6(2kD_{\parallel} \tau / m |\theta_v| h^2)^2$ , and where  $\chi = (T_+ + T_-) / (2T_+ T_-)$  and  $\delta = (T_+ - T_-) / (2T_+ T_-)$ .

The linear evolution matrix of the coupled deformation-defect system is then, in the absence of adhesive forces [ $F(\zeta) = 0$ ] and in the Fourier space

$$\begin{pmatrix} \frac{1}{\beta^2} \omega^2 + \bar{q}^4 & 1 & 0 \\ \epsilon \bar{q}^2 (\bar{Q}(\theta)^2 - 1) & \omega + 1 + \bar{Q}(\theta)^2 & 0 \\ \delta \bar{q}^2 [\bar{Q}(\theta)^2 - 1] & 0 & \omega + 1 + \bar{Q}(\theta)^2 \end{pmatrix}, \quad (21)$$

where  $\bar{q}$  is the dimensionless wave number, and  $\bar{Q}(\theta)^2 = d_x \bar{q}_x^2 + d_y \bar{q}_y^2$ . The corresponding characteristic equation writes

$$[\omega + 1 + \bar{Q}(\theta)^2] \left[ \left( \frac{1}{\beta^2} \omega^2 + \bar{q}^4 \right) [\omega + 1 + \bar{Q}(\theta)^2] \right. \\ \left. - \epsilon \bar{q}^2 [\bar{Q}(\theta)^2 - 1] \right] = 0. \quad (22)$$

Since in realistic experimental conditions (i.e., elastic waves are much faster than diffusional transport),  $c \simeq 10^5 \text{ cm s}^{-1}$ ,  $h \leq 10^{-2} \text{ cm}$ , and  $D_{\parallel} \simeq 10^{-5} \text{ cm}^2 \text{ s}^{-1}$ , one has  $\beta \gg 1$ , and the relevant root for instability is

$$\omega_1 = \epsilon \frac{\bar{Q}(\theta)^2 - 1}{\bar{q}^2} - [1 + \bar{Q}(\theta)^2]. \quad (23)$$

Hence,  $\epsilon$  plays the role of a bifurcation parameter, and the instability threshold is given by the minimum of the marginal stability curve

$$\epsilon = \bar{q}^2 \frac{\bar{Q}(\theta)^2 + 1}{\bar{Q}(\theta)^2 - 1}. \quad (24)$$

This threshold depends on the relative orientation of the laser electrical field with respect to the crystal axis. Effectively, when  $\vec{E} \parallel \vec{1}_x$ ,  $d_x = 1 \gg d_y = \exp[-2\omega E^2/3kT]$ , and instability occurs at

$$\epsilon_c = (1 + \sqrt{2})^2 \simeq 5.8, \quad q_x = q_c(0), \quad q_y = 0, \quad q_c^4 = \epsilon_c, \quad (25)$$

where  $q$  is the scaled wave number. The corresponding unscaled wavelength is thus

$$\lambda_c(0) = \frac{2\pi \sqrt{D_{\parallel}} \tau}{\epsilon_c^{1/4}}. \quad (26)$$

In fact  $\sqrt{D_{\parallel}} \tau$  is the vacancy mean free path in the subsurface layer and is of the order of half the laser wavelength. Hence, for 1  $\mu\text{m}$  laser irradiation, one finds a critical wavelength of the order of 3  $\mu\text{m}$ , in agreement with experimental observations.<sup>17</sup>

When  $\vec{E} \parallel \vec{1}_y$ ,  $d_y = 1 \gg d_x = \exp[-2\omega E^2/3kT]$ , and one has

$$\epsilon_c = (1 + \sqrt{2})^2 \simeq 5.8, \quad q_y = q_c(0), \quad q_x = 0, \quad q_c^4 = \epsilon_c, \quad (27)$$

and  $\lambda_c(\pi/2) = \lambda_c(0)$ .

On the other hand, when  $\vec{E}$  makes a  $45^\circ$  angle with  $\vec{1}_x$  and  $\vec{1}_y$ ,  $d_x = d_y = \exp[-\omega E^2/3kT] < 1$ , and the problem becomes isotropic. As a result,

$$\epsilon_c = \frac{(1 + \sqrt{2})^2}{d}, \quad \left| \vec{q}_c \left( \frac{\pi}{4} \right) \right| = \left( \frac{\epsilon_c}{d} \right)^{1/4} \quad (28)$$

and the corresponding wavelength is equal to

$$\lambda_c \left( \frac{\pi}{4} \right) = \lambda_c(0) \left( \frac{d}{\epsilon_c} \right)^{1/4}. \quad (29)$$

It is therefore apparent that, in systems where the laser electric field is parallel to one of the crystallographic axes, modes with wave vectors parallel to it are linearly selected. This leads to the growth of one-dimensional gratings perpendicular to the corresponding crystallographic axis. However, nonlinear analysis beyond instability is necessary to determine the stability of such patterns. It is also important to emphasize, for comparison with experimental observations, that, although the instability threshold is sensitive to irradiation beam orientation, the critical wavelength is only weakly sensitive to it.

For  $\alpha \neq 0$ , the situation is qualitatively the same but quantitatively different. For example,  $D_{\parallel}(\alpha) \propto P_0 \exp[(\omega E^2/3kT)(1 + \cos^2 \alpha)] \leq D_{\parallel}(0)$ , and  $d_x(\alpha, \theta) = \exp[-(2\omega E^2/3kT) \cos^2 \alpha \sin^2 \theta]$  [ $d_x(\alpha, 0) = 1$ ],  $d_y(\alpha, \theta) = \exp[-(2\omega E^2/3kT) \cos^2 \alpha \cos^2 \theta]$  [ $d_y(\alpha, \pi/2) = 1$ ], which implies that the corresponding instability threshold  $\epsilon_c(\alpha)$  is higher than for normal irradiation,  $\epsilon_c(\alpha) > \epsilon_c(0)$ . As a result instability requires higher energy irradiation, and should result in lower amplitude patterns.

In systems where the laser electric field is oriented at  $45^\circ$  with the crystallographic axis, linear terms are spatially isotropic. In this case, there is an orientational degeneracy in the

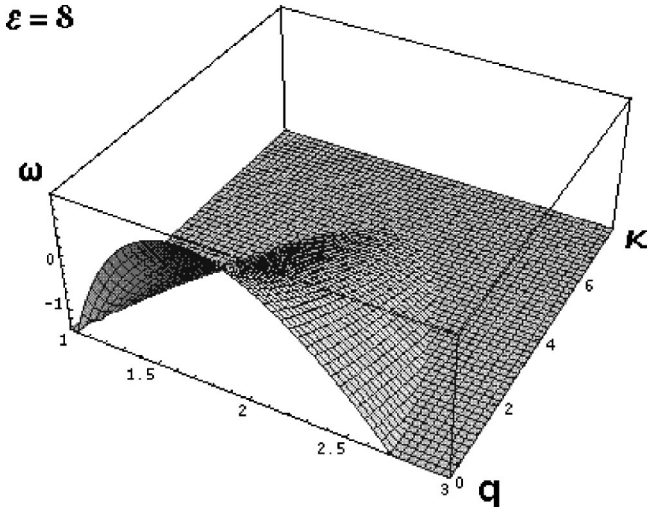


FIG. 5. Effect of adhesive forces on the linear growth rate of unstable modes. It is observed that, even above instability ( $\epsilon=8$ ,  $\epsilon_c \approx 5.8$ ), the linear growth rate becomes negative for all  $q$ , for sufficiently high adhesion.

problem, since the linear growth rate of the unstable modes only depend on  $q^2$ . Furthermore, the critical wavelength should be slightly smaller than in the previous case. Under these conditions, all unstable modes with any orientation may equally grow. The survivors, and of course the final selected patterns are then determined by their nonlinear interactions. Hence, the nonlinear saturation terms of the dynamics will determine which structure should be selected and what its stability domain should be. This study is performed in Sec. IV.

**B. Effect of adhesive forces on the instability threshold**

Adhesion between film and substrate may be modeled by a system of springs acting between every film-substrate atom pair. The corresponding force is thus proportional to the transverse film deflection  $\xi$ , the proportionality coefficient representing the stiffness of the adhesion bond. Such forces vanish beyond some cutoff value of  $\xi$ , where the film separates from the substrate, as can be seen schematically in Fig. 2. Since we are considering situations where the system is close to instability, we are dealing with small deformation profiles only, and we may thus assume the film-substrate adhesive forces to be in the linear regime. Equation (20) may thus be written as

$$\frac{1}{\beta^2} \partial_t^2 \zeta = -\bar{\Delta}^2 \zeta + u \sigma_{ij}(\zeta) \bar{\partial}_{ij}^2 \zeta - n - \bar{K} \zeta, \quad (30)$$

where  $\bar{K} = (12D_{\parallel}^2 \tau^2 / \rho c^2 h^3) K$ , and the relevant root for instability becomes

$$\omega_1 = \epsilon \bar{q}^2 \cdot \frac{\bar{Q}(\theta)^2 - 1}{\bar{q}^4 + \bar{K}} - [1 + \bar{Q}(\theta)^2]. \quad (31)$$

It is easy to see that adhesive forces stabilize the system, and may even suppress instability, as shown on Fig. 5, where

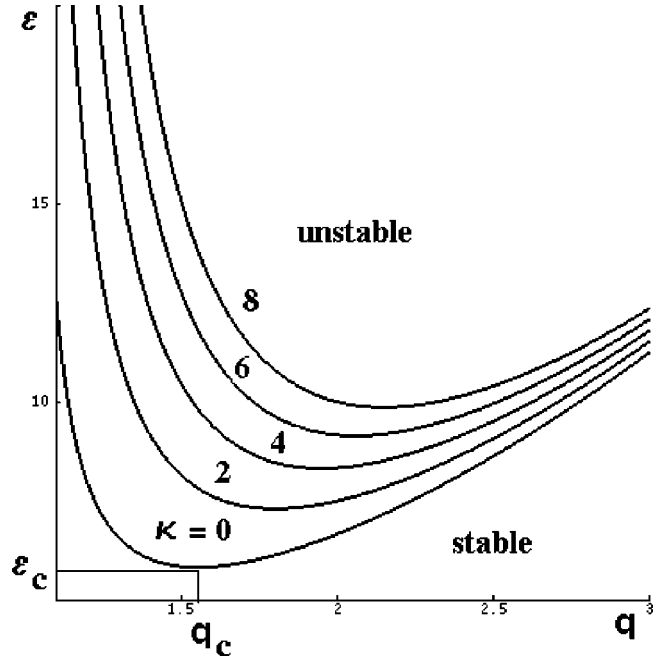


FIG. 6. Marginal stability curves for increasing values of adhesion intensity  $\bar{K}$ , showing an increase of the instability threshold, and hence stabilization of the undeformed film surface for increasing adhesion.

linear growth rate becomes negative for increasing adhesive force stiffness. The increase of marginal stability curve, instability threshold and critical wave number with adhesion intensity is shown on Fig. 6.

On the other hand, unstable modes, with critical wave number  $q_c = \epsilon^{1/4}$ , are stabilized for  $\bar{K} > \epsilon - \epsilon_c$ . More generally, for any  $\epsilon > \epsilon_c$ , instability is suppressed, and undeformed surfaces remain stable, for well defined values of  $\bar{K} = \bar{K}(\epsilon)$ , as shown in Fig. 6.

**IV. WEAKLY NONLINEAR ANALYSIS AND PATTERN SELECTION**

In the weakly nonlinear regime beyond a pattern forming instability, the dynamics may be reduced to the evolution of an order parameterlike variable which corresponds to the unstable modes.<sup>28</sup> This reduction may be performed in the framework of the adiabatic elimination of the stable modes.<sup>29</sup> In the present case, one is the total mean defect density  $N$  which is the eigenmode corresponding to the eigenvalue  $\omega = -[1 + \bar{Q}(\theta)^2]$  of the linear evolution matrix. The second one is the transverse displacement of the midplane  $\zeta$  that may also be adiabatically eliminated since the characteristic time scale of its evolution  $\beta$  is negligably small. These two variables may thus be expressed, in Fourier transform, as a series expansion in powers of  $n$ .

**A. Isotropic surface deformation patterns**

When the electric field is oriented at  $45^\circ$  with atomic bonds,  $\bar{Q}(\theta)^2 = d\bar{q}^2$ , and the system behaves isotropically. In

this case, one recovers, in the absence of adhesive forces ( $\bar{K}=0$ ) the situation described in Ref. 9, where the evolution equation for an order parameter such as  $n_{\vec{q}}$  is, in the weakly nonlinear regime around the instability

$$\begin{aligned} \tau_0 \partial_T n_{\vec{q}} = & [\bar{\epsilon} - \Lambda(q^2 - q_c^2)] n_{\vec{q}} + v \int_c d\vec{k} (\vec{1}_{\vec{q}} \cdot \vec{1}_{\vec{k}}) n_{\vec{q}-\vec{k}} n_{\vec{k}} \\ & - \int_c d\vec{k} \int_c d\vec{k}' w(\{\vec{1}_{\vec{q}}\}) n_{\vec{q}-\vec{k}-\vec{k}'} n_{\vec{k}} n_{\vec{k}'} + \dots, \end{aligned} \quad (32)$$

where  $\tau_0 = (2 + \sqrt{2})^{-1}$ ,  $\bar{\epsilon} = (\epsilon - \epsilon_c) / \epsilon_c$ ,  $\Lambda = \tau_0 / dq_0^2$ ,  $v = \tau_0 (\delta + \chi \eta / \epsilon_c)$  and

$$\begin{aligned} w = & \frac{u}{q_0^8} \sum_{i,j} E_{ij}(\{\vec{1}_{\vec{q}}\}) + \tau_0 \chi \left( \chi + \frac{\delta \eta}{\epsilon_c} \right) (\vec{1}_{\vec{q}} \cdot \vec{1}_{\vec{k}}) \\ & \times [(\vec{1}_{\vec{q}} - \vec{1}_{\vec{k}}) \vec{1}_{\vec{k}'}] \frac{d^2}{1 + 2dq_0^2 [1 - (\vec{1}_{\vec{q}} \cdot \vec{1}_{\vec{k}})]}, \end{aligned} \quad (33)$$

$$\gamma(\psi) = \frac{4d^2 \cos^2(\psi) / [(1 + 2dq_0^2)^2 - 4dq_0^4 \cos^2(\psi)] + \bar{u} [2\nu + 2(1 - \nu) \cos^2(\psi)]}{2/(1 + 4dq_0^2) + \bar{u}}. \quad (37)$$

On the other hand, squares exist for all  $\bar{\epsilon} > 0$ , but are unstable versus hexagons in the range  $0 \leq \bar{\epsilon} \leq \epsilon_h$ , with

$$\epsilon_h = \frac{v^2}{2w_0 [\gamma(2\pi/3) + \gamma(\pi/6)]}.$$

Both patterns are simultaneously stable for  $\bar{\epsilon} > \epsilon_h$ .

Hence, since squares are unstable close to instability, hexagonal deformation patterns should always be observed first for a steady increase of laser intensity. For “quench” experiments, i.e., when laser irradiation is initiated suddenly in the range  $\bar{\epsilon} > \epsilon_h$ , either squares or hexagons could be selected, as a result of their bistability.

### B. Anisotropic surface deformation patterns

When the electric field is parallel to one of the crystallographic axes, the system behaves anisotropically. Consider now the case where  $\vec{E} \parallel \vec{1}_x$ ,  $d_x = 1 \gg d_y$ , and  $\bar{Q}^2 = q_x^2 + d_y q_y^2$

$$\begin{aligned} \tau_0 \partial_T n_{\vec{q}} = & [\bar{\epsilon} - \Lambda_a(q^2 - q_c^2)^2 - \Delta q_y^2] n_{\vec{q}} \\ & - \int_c d\vec{k} \int_c d\vec{k}' w_a(\{\vec{1}_{\vec{q}}\}) n_{\vec{q}-\vec{k}-\vec{k}'} n_{\vec{k}} n_{\vec{k}'} + \dots, \end{aligned} \quad (38)$$

where  $\Lambda_a = \tau_0 / q_c^2$ ,  $\Delta = (1 - d_y) / (1 + \sqrt{2})$ , and

where  $q_0 = q_c(\pi/4)$ . It has been found<sup>9</sup> that, for sufficiently thin films, selected patterns correspond to square or hexagonal planforms. Hexagons exist and are stable in the range<sup>30</sup>

$$- \frac{v^2}{16w_0 \left[ 1 + 2\varpi \left( \frac{2\pi}{3} \right) \right]} \leq \bar{\epsilon}, \quad (34)$$

where

$$\begin{aligned} w_0 = & \frac{u}{q_0^8} + \frac{2d^2}{1 + 4dq_0^2} \tau_0 \chi \left( \chi + \frac{\delta \eta}{\epsilon_c} \right) \\ = & \tau_0 \chi \left( \chi + \frac{\delta \eta}{\epsilon_c} \right) \left( \bar{u} + \frac{2d^2}{1 + 4dq_0^2} \right) \end{aligned} \quad (35)$$

with

$$\bar{u} \approx \frac{12}{\tau_0 d^2} \left( \frac{2kTD_{\parallel} \tau}{q_0^4 |\theta_v| h^2} \right)^2 \quad (36)$$

and

$$\begin{aligned} w_a = & \frac{u}{q_0^8} \sum_{i,j} E_{ij}(\{\vec{1}_{\vec{q}}\}) + \tau_0 \chi \left( \chi + \frac{\delta \eta}{\epsilon_c} \right) \\ & \times \frac{(q_x k_x + d_y q_y k_y) [(q - k)_x k'_x + d_y (q - k)_y k'_y]}{k^2 k'^2 [1 + (q - k)_x^2 + d_y (q - k)_y^2]}. \end{aligned} \quad (39)$$

Linear terms favor one-dimensional modulations with  $q_x = q_c$  and  $q_y = 0$ , while nonlinear terms favor square planform. Effectively, in this case also,  $\gamma(\psi)$  is minimum for  $\psi = \pi/2$  and  $\gamma(\pi/2) \approx 2u\nu / (1 + u) \ll 1$ , since  $\nu \ll 1$  for such films. Pattern selection may thus be studied with amplitude equations for modulations along  $x$  and  $y$  directions.<sup>29</sup> For uniform amplitudes, one has

$$\begin{aligned} n_{\vec{q}} \propto & A(T) e^{iq_c x} + A^*(T) e^{-iq_c x} + B(T) e^{iq_c y} \\ & + B^*(T) e^{-iq_c y} + \dots \end{aligned}$$

$$\tau_0 \partial_T A = \bar{\epsilon} A - w_0 A \left[ |A|^2 + \gamma \left( \frac{\pi}{2} \right) |B|^2 \right] + \dots$$

$$\tau_0 \partial_T B = [\bar{\epsilon} - \Delta q_c^2] A - w_0 B \left[ |B|^2 + \gamma \left( \frac{\pi}{2} \right) |A|^2 \right] + \dots \quad (40)$$

From these equations, it results that gratings perpendicular to the  $x$  direction and of amplitude  $|A_g|^2 = \bar{\epsilon}$  ( $B=0$ ) are stable

in the domain  $0 < \bar{\epsilon} < \Delta q_c^2 / (1 - \gamma) \approx 1$  or  $(1 + \sqrt{2})^2 \approx 5.8 < \mu(C_+ / T_+ + C_- / T_-) \leq 11.6$ . For  $\bar{\epsilon} > \Delta q_c^2 / (1 - \gamma)$ , one-dimensional gratings become unstable versus square patterns of amplitude  $|A_s|^2 = |B_s|^2 = \bar{\epsilon} / (1 + \gamma)$ .

For nonparallel orientation of the electric field (e.g., for arbitrary  $\theta$  such that  $d_x > d_y$ ), gratings perpendicular to the  $x$  direction ( $2 = 1 = 4$  bonds) are still selected at instability, but their stability domain  $0 < \bar{\epsilon} < \Delta q_c^2 / (1 - \gamma) \approx 1$  is reduced, since  $\Delta(\theta < \pi/4) \propto d_x - d_y < \Delta(0)$ . For  $\pi/4 < \theta < 3\pi/4$ , gratings perpendicular to the  $y$  direction ( $3 = 1 = 5$  bonds) are selected at threshold.

Although adhesive forces lower instability thresholds, as discussed previously, they do not affect qualitatively pattern selection and stability. Effectively, they do not modify the angular dependence of nonlinear couplings, as it may easily be seen, for example, in the anisotropic case, where one has

$$w_{\text{adh}} = \frac{uq^4}{(q^4 + \bar{K})^3} \sum_{i,j} E_{ij}(\{\tilde{I}_q\}) + \tau_0 \chi \left( \chi + \frac{\delta\eta}{\epsilon_c} \right) \times \frac{(q_x k_x + d_y q_y k_y) [(q-k)_x k'_x + d_y (q-k)_y k'_y] k^2 k'^2}{(k^4 + \bar{K})(k'^4 + \bar{K}) [1 + (q-k)_x^2 + d_y (q-k)_y^2]}.$$

Previous results remain also qualitatively valid for non-normal irradiation ( $\alpha \neq 0$ ), since, although  $d_x$  and  $d_y$  explicitly depend on  $\alpha$  and  $\theta$ , the sign of  $d_x - d_y$ , which determines the orientation of the gratings selected at instability, only depends on the angle  $\theta$  between the projection of the electric field and atomic bonds on the surface plane (100). However, the stability range of these gratings explicitly depends on  $d_x - d_y$  and thus on  $\alpha$ . In the limiting case of irradiation parallel to the surface, the  $\theta$  dependence of diffusion constants vanishes. The system becomes isotropic, irrespective of the in-plane irradiation orientation, and two-dimensional cellular deformation patterns should be selected.

## V. COMPARISON WITH EXPERIMENTS

The results of experimental studies of laser irradiation of single crystal silicon wafers have been reported in Refs. 17,18. On increasing laser intensity in normal irradiation, the following succession of patterns has been reported. Below a threshold corresponding to laser fluence of  $8.5 \text{ J cm}^{-2}$  (for an Nd-YAG laser providing 1.6 ms pulses of polarized radiation at  $\lambda = 1.06 \text{ } \mu\text{m}$ ), no surface deformation has been observed. Above this threshold, two-dimensional cellular structures, with no dependence of the orientation of this structure on laser polarization, have been observed. For a further increase of the laser intensity, the authors report observation of structures depending on the relative orientation of the polarization vector of the laser beam and crystallographic axes. When the electric field is oriented along one of the crystallographic axes, one-dimensional gratings perpendicular to this axis, with a period  $\lambda_1$  of the order of  $3 \text{ } \mu\text{m}$ , is formed at the film surface. When the electric field is oriented at an angle of  $45^\circ$  with respect to the crystallographic axis, two-dimensional gratings perpendicular to the crystallographic axis are formed, with the same period.

When the incident laser beam is not normal to the surface, a similar succession of structures as the ones described above has been observed. However, in addition to the structures described previously, new gratings, with wavelength,  $\lambda_2$ , depending on the incidence angle, and perpendicular to the electric field were observed. The wavelength variation law  $\lambda_2 = \lambda / (1 - \sin \alpha)$  suggests that these structures correspond to interferential gratings<sup>19</sup> and are out of the scope of the present study. One should note, however, that the contrast between deformational and interferential gratings decreases when the incidence angle increases. It indicates that the amplitude of deformational patterns decreases for increasing  $\alpha$ .

Several of these observations are in agreement with our findings. The dynamical model studied in this paper predicts the formation of laser induced deformation patterns on the film surface above a well-defined threshold. When the interaction between the electric field and atomic bonds is weak, the system is isotropic and two-dimensional cellular patterns with no definite orientation have been predicted and studied in Ref. 9. For a sufficiently intense electric field so as to break covalent bonds, orientational effects appear. In this case, when the field is parallel to one of the crystallographic axes, one-dimensional gratings perpendicular to it are predicted. Nevertheless, on increasing the irradiation intensity, one-dimensional gratings should become unstable versus two-dimensional orthogonal gratings. This effect has not been reported yet although such two-dimensional gratings have been observed when the electric field is oriented at an angle of  $45^\circ$  with respect to the  $[110]$  crystallographic axis, in agreement with our analysis. For increasing incidence angles, our analysis does not predict qualitative changes for pattern selection, in agreement with experimental observations. The observed decrease in pattern amplitude could correspond to the predicted increase of the critical defect density.

Adhesion forces are expected to stabilize undeformed surfaces and could even be able to suppress deformational instabilities. Unfortunately, and to our knowledge, no systematic experimental analysis of adhesion effects is available. Quantitative predictions may easily be obtained regarding the minimum level of adhesion force required to stabilize the deformation of the thin film, but more systematic experimental studies are needed to allow for detailed comparisons with this theory, especially in the presence of adhesive forces.

In physical variables, the deformation instability threshold for weakly adherent films is given by

$$\epsilon_c = \frac{6m\theta_v^2 D_{\parallel} \tau}{\rho c^2 h^2 k} \left( \frac{C_+}{T_+} + \frac{C_-}{T_-} \right) \Bigg|_c \approx 5.8. \quad (41)$$

Comparing to the experimental conditions of Ref. 18, this corresponds to a vacancy density of the order of  $C_+ \approx 5 \times 10^{18} \text{ cm}^{-3}$ , or a film top surface temperature  $T_+$  of about  $1000 \text{ K}$  ( $\approx 0.7T_m$ ). This temperature is given by<sup>9</sup>

$$T_+ \approx \frac{I_0(1-R)h}{\kappa}, \quad (42)$$

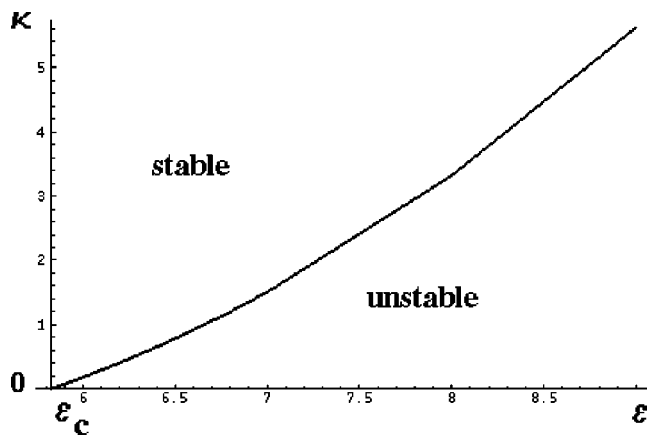


FIG. 7. Adhesion bonding stiffness  $\bar{K}$ , necessary to suppress the surface deformation instability, as a function of the bifurcation parameter  $\epsilon$ .

where  $I_0$  is the laser power density,  $R$  the surface reflectivity, and  $\kappa$  the thermal conductivity. In the case of Si, where  $R \approx 0.3$ ,  $\kappa \approx 0.1$  W/cm K, and  $h = 0.01$  cm, this temperature corresponds to a laser power of the order of  $10^4$  W/cm<sup>2</sup>. For the laser used in Ref. 18 with pulses of 1.6 ms, this corresponds to a critical laser energy density of the order of 15 J/cm<sup>2</sup>, which is in the range of fluences where deformation patterns have been experimentally observed.<sup>18</sup>

It is interesting to note that if one considers SiC single crystals, it has higher reflectivity, thermal conductivity and melting point as compared to Si. If one uses the value of  $\kappa \approx 4.9$  W/cm K for SiC, the predicted critical laser energy density that is necessary to induce surface deformational instabilities would be at least 200 J/cm<sup>2</sup>. Therefore, and according to the present model, SiC is expected to be considerably more resistant to laser damage than Si.

As far as adhesive forces are concerned, one can see from Fig. 7 that adhesive forces with scaled stiffness constant of the order of 2 would suppress the deformation instability at  $\epsilon = 7.5 > \epsilon_c$ . This implies that the corresponding unscaled stiffness constant is  $K = \rho c^2 h^3 / 6 D_{\parallel}^2 \tau^2 \approx 10^{10}$  MPa/m. For a film-substrate separation distance of the order of a lattice constant, this stiffness would correspond to adhesive forces of the order of 25 MPa.

## VI. CONCLUSIONS

The study of laser induced deformation patterns in thin films has been performed in the case of covalent solid films with varying degrees of adhesion with the substrate. In this case, the interaction between the electric field and covalent bonds may lift the orientational degeneracy of unstable modes since their linear growth rate becomes dependent on the electric field orientation relative to crystallographic directions.

However, pattern symmetry, selection and stability depends on the interplay between linear growth rates and nonlinear couplings between unstable modes. In the present case, linear anisotropy induced by bond breaking favors the formation of one-directional gratings while nonlinear terms favor two-dimensional cellular patterns. The results of pattern selection analysis have been compared to experimental observations. The following significant conclusions from the present analysis are obtained.

(1) Adhesion forces reduce linear growth rates of unstable modes, and may even suppress instability when they are sufficiently strong.

(2) For weak electric fields, which are not sufficient to induce bond breaking, two-dimensional patterns without preferred orientation are formed.

(3) For strong electric fields, bond breaking increases the defect mobility along  $\langle 110 \rangle$  directions. One-dimensional gratings perpendicular to these directions develop in the weakly nonlinear regime. For stronger nonlinearities, these gratings should transform to two-dimensional gratings with specific orientations.

(4) Deformation patterns depend only quantitatively on the incidence angle of the laser radiation with respect to the film surface.

(5) As a result of its higher thermal conductivity, reflectivity and melting point as compared to Si, the LIDT for deformational surface instabilities in SiC is predicted to be considerably higher than the Si case, and may be in excess of 200 J/cm<sup>2</sup>.

## ACKNOWLEDGMENTS

Financial support of the U.S. Department of Energy (DOE) through Grant No. DE-FG03-00ER54594 with UCLA is gratefully acknowledged. D.W. has also been supported by a grant of the Belgian National Fund for Scientific Research.

<sup>1</sup>O. Ueda, J. Electrochem. Soc. **145**, 11 (1988).

<sup>2</sup>S. C. Jones, P. Braunlich, R. T. Casper, X.-A. Shen, and P. Kelly, Opt. Eng. (Bellingham) **28**, 1039 (1989).

<sup>3</sup>C. V. Shank, R. Yen, and C. Hirlimann, Phys. Rev. Lett. **50**, 454 (1983).

<sup>4</sup>H. W. K. Tom, G. D. Aumiller, and C. H. Brito-Cruz, Phys. Rev. Lett. **60**, 1438 (1983).

<sup>5</sup>T. Schroeder, W. Rudolph, S. V. Govorkov, and I. L. Shumay, Appl. Phys. A: Solids Surf. **51**, 49 (1990).

<sup>6</sup>M. Bertolotti, G. Vitali, and U. Zammit, *Laser and Electron Beam Interactions with Solids*, edited by B. R. Appleton and G. K. Celler (North-Holland, Amsterdam, 1982), Vol. 4, p. 203.

<sup>7</sup>G. K. Celler, J. Cryst. Growth **63**, 429 (1983).

<sup>8</sup>D. Bauerle, *Chemical Processing with Lasers*, Springer Series in Materials Science (Springer-Verlag, Berlin, 1986).

<sup>9</sup>D. Walgraef, N. M. Ghoniem, and J. Lauzeral, Phys. Rev. B **56**, 15 361 (1997).

<sup>10</sup>C. Cohen-Tannoudji, B. Diu, and F. Laloe, *Quantum Mechanics* (Wiley, New York, 1992).

<sup>11</sup>R. Kossowsky and S. C. Singhal, *Surface Engineering, Surface Modification of Materials* (Martinus Nijhoff, Dordrecht, 1984).

<sup>12</sup>L. Laude, D. Bauerle, and M. Wauthélet, *Interfaces under Laser Irradiation* (Martinus Nijhoff, Dordrecht, 1987).

<sup>13</sup>D. Walgraef and N. M. Ghoniem, *Patterns, Defects and Materials*

- Instabilities* (Kluwer Academic, Dordrecht, 1990).
- <sup>14</sup>R. Mc Connell and R. Noufi, *Science and Technology of Thin Film Superconductors* (Plenum, New York, 1990).
- <sup>15</sup>J. S. Preston, J. E. Sipe, and H. R. van Driel, in *Interfaces under Laser Irradiation*, edited by L. Laude, D. Bauerle, and M. Wauthelet (Martinus Nijhoff, Dordrecht, 1987), pp. 127–136.
- <sup>16</sup>P. K. Kasharov and V. F. Kiselev, *Izv. Akad. Nauk SSSR, Ser. Fiz.* **50**, 435 (1986).
- <sup>17</sup>V. I. Emel'yanov, *Laser Phys.* **2**, 389 (1992).
- <sup>18</sup>A. F. Banishev, V. I. Emel'yanov, and M. M. Novikov, *Laser Phys.* **2**, 192 (1992).
- <sup>19</sup>J. F. Young, J. S. Preston, and H. R. van Driel, *Phys. Rev. B* **27**, 1141 (1983); **27**, 1155 (1983).
- <sup>20</sup>J. Lauzeral, D. Walgraef, and N. M. Ghoniem, *Phys. Rev. Lett.* **79**, 2706 (1997).
- <sup>21</sup>D. Walgraef, *J. Eng. Mater. Technol.* **121**, 182 (1999).
- <sup>22</sup>R. M. Wood, *Laser Damage in Optical Materials*, The Adam Hilger Series on Optical and Optoelectronics (Bristol, London, 1986), p. 27.
- <sup>23</sup>H. E. Bennett, A. H. Guenther, M. R. Kozlowski, B. E. Newnam, and M. J. Soileau, *27th Annual Boulder Damage Symposium: Laser-Induced Damage in Optical Materials*, Proc. SPIE **2714** (1995).
- <sup>24</sup>A. Needleman, *Int. J. Fract.* **42**, 21 (1990).
- <sup>25</sup>X. P. Xu and A. Needleman, *Int. J. Fract.* **74**, 289 (1996).
- <sup>26</sup>T. Siegmund, N. A. Fleck, and A. Needleman, *Int. J. Fract.* **85**, 381 (1997).
- <sup>27</sup>L. D. Landau, *Theory of Elasticity* (Pergamon Press, Oxford, 1986).
- <sup>28</sup>M. C. Cross and P. C. Hohenberg, *Rev. Mod. Phys.* **65**, 851 (1993).
- <sup>29</sup>D. Walgraef, *Spatio-Temporal Pattern Formation (With Examples in Physics, Chemistry and Materials Science)* (Springer Verlag, New York, 1996).
- <sup>30</sup>P. Borckmans, G. Dewel, A. De Wit, and D. Walgraef, in *Chemical Waves and Patterns*, edited by R. Kapral and K. Showalter (Kluwer, Dordrecht, 1994), pp. 323–363.